Flexible Nanofiber-Reinforced Aerogel (Xerogel) Synthesis, Manufacture, and Characterization

Lichun Li,[†] Baris Yalcin,[†] Baochau N. Nguyen,[‡] Mary Ann B. Meador,[§] and Miko Cakmak*[,†]

Polymer Engineering Department, The University of Akron, 250 S. Forge Street, Akron, Ohio 44325-0301, Ohio Aerospace Institute, 22800 Cedar Point Road, Cleveland, Ohio 44111, and NASA Glenn Research Center, 21000 Brookpark Road, Cleveland, Ohio 44135

ABSTRACT Silica aerogels are sol−gel-derived materials consisting of interconnected nanoparticle building blocks that form an open and highly porous three-dimensional silica network. Flexible aerogel films could have wide applications in various thermal insulation systems. However, aerogel thin films produced with a pure sol−gel process have inherent disadvantages, such as high fragility and moisture sensitivity, that hinder wider applications of these materials. We have developed synthesis and manufacturing methods to incorporate electrospun polyurethane nanofibers into the cast sol film prior to gelation of the silica-based gel in order to reinforce the structure and overcome disadvantages such as high fragility and poor mechanical strength. In this method, a two-stage sol−gel process was employed: (1) acid-catalyzed tetraethyl orthosilicate hydrolysis and (2) base-catalyzed gelation. By precisely controlling the sol gelation kinetics with the amount of base present in the formulation, nanofibers were electrospun into the sol before the onset of the gelation process and uniformly embedded in the silica network. Nanofiber reinforcement did not alter the thermal conductivity and rendered the final composite film bendable and flexible.

KEYWORDS: hybrid film • silica aerogel • electrospinning • nanofiber embedding • polyurethane • flexible superinsulator

1. INTRODUCTION

Aerogel is a solid formed by supercritical fluid (SCF) extraction of a gel resulting in a porous open cell solid with a thermal conductivity as low as 0.013 W/m · K (1). Silica aerogels are highly porous materials with large internal surface area, low density, and large pore volume. They exhibit high impedance to acoustic waves, a low dielectric constant, and extremely low thermal conductivity. Low-density aerogel materials (0.01−0.3 g/cm^3) are widely considered to be excellent thermal insulators. Aerogels function as thermal insulators primarily by minimizing conduction (low density and a tortuous path for heat transfer through the solid nanostructure), convection (very small pore sizes minimize convection), and radiation with added IR-absorbing or -scattering dopants in the aerogel matrix. Aerogels are synthesized by a sol−gel process (2) and dried under SCF extraction/exchange conditions (3, 4). The SCF drying process involves solvent exchange of gelation solvents filling the mesopores with liquid CO_2 in an autoclave with subsequent supercritical CO_2 venting. The supercritical phase in SCF drying eliminates the liquid/vapor interface inside the pore, avoiding the formation of capillary pressure, which collapses the network.

Consequently, without surface tension forces exerted on the skeletal framework, SCF drying leaves the geometric dimensions of the wet gel unaffected, resulting in low-density materials with high porosity.

Chemically, sol−gel reactions can be viewed as a two-step network-forming polymerization. The first step is the hydrolysis of metal alkoxides to generate intermediate species. These species then undergo a stepwise polycondensation reaction to form a three-dimensional network. Both the hydrolysis and polycondensation reactions can be catalyzed by acid or base. In acid catalysis conditions, the rate of hydrolysis is faster than the rate of polycondensation. Primary particles are formed, and the resultant silica exhibits a highly ramified, low fractal-dimensional structure (5). On the other hand, in the presence of a base catalyst, the rate of condensation is faster than that of hydrolysis, which results in the formation of dense, colloidal particles (5). In a two-stage acid−base sol−gel process (6, 7), the hydrolysis of a silicate monomer is catalyzed by an acid catalyst, and then the polycondensation of colloidal particles is catalyzed by a base catalyst, leading to the buildup of a systematic, complete, and continuous network.

Sol−gel reactions form the basis for aerogel film formation (8). In a typical aerogel film-forming process, an ungelled precursor sol is cast/deposited onto a substrate to form the film, gelled, and dried into a dense form. The precursor sol comprises a stock solution, a volatile solvent, and a gelation catalyst that modifies the pH of the sol to speed gelation. During and after casting and/or deposition, the volatile components in the sol film are allowed to rapidly evaporate to facilitate the gelation. The aerogel film pro-

* Corresponding author. Tel: 330972 6928. Fax: 330258 2339. E-mail: cakmak1@uakron.edu.
Received for review July 2, 2009 and accepted October 13, 2009
[†] The University of Akron.
[‡] Ohio Aerospace Institute.
[§] NASA Glenn Research Center.
DOI: 10.1021/am900451x

duced with this pure sol−gel process has inherent fragility, which hinders wider applications of these materials (9). The aerogel fragility is ultimately traced to their structure. Nanoscopically, silica aerogels prepared through an acid−base-catalyzed sol−gel route consist of a "pearl-necklace-like" fractal network of secondary silica nanoparticles with dimensions of about 5−10 nm (4). The fragility of the aerogel framework is traced to the interparticle connecting zones, referred to as necks. Necks are formed by the coagulation of particles upon gelation and grow to a certain point by dissolution and reprecipitation of silica during aging of freshly made gels. The interparticle necks are the well-defined weak points that cause mechanical failure when stress is applied on the material, leading to fracture occurring at the interface of secondary particles (necks), while primary particles remain intact. Hence, it is reasonable that when the interparticle necks are rendered wider, the specific strength of silica aerogels can be improved without incurring a severe weight penalty. In this respect, by bridging nanoparticles with a cross-linking procedure (10), the performance of the silica aerogel thin film in terms of strength and modulus can be improved. In the cross-linking method, silica particles with surface-terminated silanol (11) or amine groups are cross-linked with diisocyanate, forming polyurea (12−15), or with epoxide, forming epoxy resin (16). The amine-modified silica particles can also be functionalized with styrene, leading to polystyrene cross-linking within the silica network (17). In addition to the method of cross-linking secondary silica particles with covalent chemical bonds, it has also been reported that the mechanical properties of silica aerogel were enhanced by templating the aerogel network structure development with the dropwise addition of colloidal polystyrene into the sol prior to gelation (18).

Recently, doping silica aerogel with various types of fibers as a skeleton-supporting material to increase the mechanical properties of aerogels has become an attractive topic in the field of the aerogel preparation area. With respect to the nanofiber reinforcement method, there are three categories: (1) Nanofibers were mixed into the sol prior to the onset of gelation and incorporated in the wet gel with the completion of gelation. In this category, it has been reported that the incorporation up to 5% carbon nanofiber in low-density diisocyanate cross-linked silica aerogel monoliths provides as much as 5-fold improvement in the tensile strength, compared to the unreinforced aerogels (19); an additional case in this category is that the mechanical strength of the silica aerogel doped with 10% ceramic fibers was improved 6 times over that of the pure silica aerogel (20). (2) Scientists at Aspen Aerogels Inc. have recently reported that the thermal and mechanical performances were improved with fiber-reinforced aerogel composites (21). In this category, the aerogel composites are primarily composed of two parts, namely, a reinforcing continuous nonwoven fiber batting and an aerogel matrix. This type of aerogel composite was made by pouring the silica precursor solution on top of a lofty fiber batting blanket previously placed in a container and allowing gelation to occur within a few minutes by the slow addition of catalyst. With aging and subsequent CO_2 SCF drying, a "blanket gel" was rendered. (3) In this report, we first designed a *continuous* electrospun nanofiber reinforcement method, in which the nanofiber made from a polyurethane (PU)-containing poly(dimethylsiloxane) (PDMS) as the soft segment (22) is electrospun into the cast sol film and incorporated into the film during the gelation process (23).

An electrospinning technique is an effective method to produce nanofibers (24−29). The process of electrospinning involves the application of a strong electrostatic field to a capillary spinneret with a metallic needle connected to a reservoir containing a polymer solution or melt. Under the influence of the electrostatic field, a pendant droplet of the polymer solution at the capillary tip is deformed into a conical shape (Taylor cone). If the voltage surpasses a threshold value, electrostatic forces overcome the surface tension, and a fine charged jet is ejected. The jet moves toward a ground plate acting as a counter electrode, which in our case is the thin cast sol film. The viscosity of the polymer solution plays an important role in the electrospinning process. Too low viscosity results in the electrospraying process producing nanosized droplets. If the extensional viscosity is sufficiently high, the polymer solution forms a stable thread. The solvent begins to evaporate immediately after the jet is formed. The result is the deposition of a thin polymer fiber into the cast sol. In the nanofiber electrospun reinforcement method, the silica network works as a matrix and the uniformly distributed nanofibers function as a skeleton to reinforce and support the inherent fragile silica network. In addition, nanofibers are expected to alleviate the capillary pressure during the drying process, to adjust the pore sizes of the gel network, and to add flexibility to the gel network.

In this work, for the first time we designed and constructed a process where we prepared a PDMS hybrid silica aerogel (xerogel) thin film reinforced by continuous electrospun nanofibers. In this method, the fragility of the aerogel material is reduced by reinforcing the mesoporous structure in three dimensions: perpendicularly, by macroscopically electrospinning nanofibers into the silica aerogel matrix along with microscopically interconnecting interparticle necks within the mesoporous silica network on the planar dimension by cross-linking the silica particles with a silanol-terminated PDMS oligomer to modify the brittleness and stiffness of the silica matrix. The electrospinning nanofiber reinforcement was accomplished through the electrospinning of nanofibers into the sol whose gelation kinetics were delayed so that the nanofibers can easily penetrate the cast wet sol film while it is still exhibiting low viscosity. The controlled gelation kinetics of the sol ensures that nanofibers are embedded in the gel film or at least anchored to it, creating continuous nanofiber reinforcements to improve the mechanical properties.

2. EXPERIMENTAL SECTION

2.1. Process. In this process (Scheme 1), the mixed sol with the desired viscosity is cast into film form on top of a nanofiber

Scheme 1. Fabrication Process of a Silica Aerogel Thin Film Reinforced by Nanofiber Electrospinning

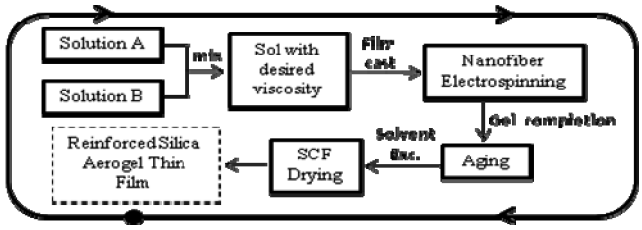

mat to prepare a sol-impregnated nanomat, which, in turn, is in situ embedded with electrospun nanofibers by the direct electrospinning of fibers onto it. This procedure was repeated three or four times to form a multilayer film with nanofibers incorporated throughout the thickness of the final composite. For the in situ embedding stage, the gelation kinetics of the sol were delayed to exhibit low viscosity so that nanofibers can easily penetrate it. The final composite is aged and dried.

The hybrid film manufacturing platform (30) that combines a multinozzle electrospinning platform integrated onto a solution-casting line is shown in Figure 1. The platform consists of several stages with individually controlled spinnerets. Each spinneret has a dedicated Teflon container, pressure/vacuum line, high-voltage power supply, disposable needles, and valves. Each spinneret is held by a holder that has $X-Y$ and Z motion capability and hence can be set at relative distances to each other. This, along with dedicated pressure/vacuum line and high-voltage power capability, allows different materials to be spun and/or sprayed simultaneously, leading to various complex composite nanostructures. Each group of spinnerets is held by a linear actuator that rasterizes the width of the cast film or any carrier moving underneath the multinozzle spinning/spraying platform. We prepared nanofiber mats and impregnated them with the sol as well as produced nanofiber embedded films in situ.

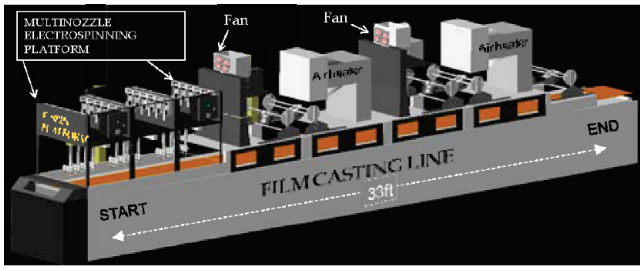

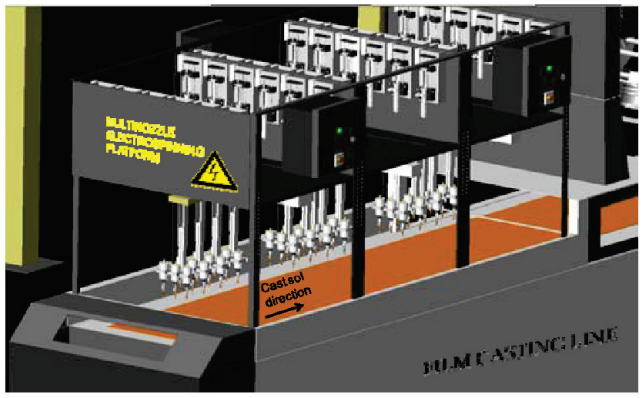

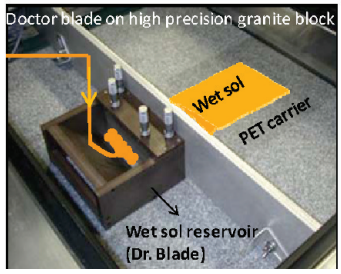

FIGURE 1. Manufacturing platform: (a) full view of the film-casting line equipped with a multinozzle electrospinning platform; (b) multinozzle spinning area; (c) wet sol casting.

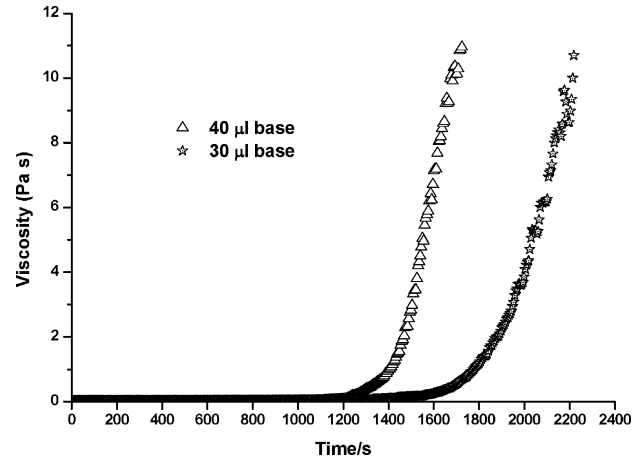

FIGURE 2. Base-catalyzed TEOS/glycerol/ethanol sol gelation kinetics.

2.2. Materials. Tetraethyl orthosilicate (TEOS), glycerol, and ethanol were purchased from the Aldrich Chemical Co. and used without further purification. The PDMS-based polyurethane (PU; Elast-Eon TM-E2A) used for nanofiber electrospinning was donated by AorTech International plc. Silanol-terminated PDMS oligomers were perchased from Gelest and used without further purification.

2.3. Sol–Gel Process. The sol–gel process employed in this research is in two stages: (i) acid-catalyzed TEOS hydrolysis and (ii) base-catalyzed gelation. The gelation kinetics can be controlled by the amount of base present in the formulation. The nanofiber electrospinning process was done in air without solvent atmosphere control; the pore collapse during the solvent evaporation was minimized by employing a multisolvent system (glycerol/ethanol).

Preparation of a TEOS Sol Solution. A total of 7.2 mL (32.3 mmol) of TEOS was dissolved in 7.2 mL (97.73 mmol) of glycerol in a 100 mL three-neck, round-bottomed flask, which was equipped with a reflux condenser. The acid catalyst solution prepared by dissolving 0.25 mL of 1 M HCl in 2.0 mL of deionized (DI) H_2O was added slowly into the TEOS/glycerol solution with vigorous stirring of the mixture for 10 min. The resultant solution was refluxed at 65 °C for 1.5 h. After the stock solution was allowed to cool to room temperature, 15 mL (248.4 mmol) of absolute ethanol and 18.4 mL (23.0 g, 250.0 mmol) of glycerol were added to adjust the viscosity of the resultant reaction mixture. The total volume of the stock solution was 49.6 mL, and the acid (1 M HCl)/TEOS molar ratio was 7.7×10^{-3}.

Gelation with Solution B (Base Catalysis) Catalysis. The gelation time of the sol was tested on a Gemini HR nano rheometer. A total of 30 and 40 μL of NH_4OH (1 M in ethanol) was added into two 2 mL sol samples, respectively, to test how the amount of base catalyst affects the gelation time. As shown in Figure 2, as the amount of base increased from 30 to 40 μL, the gelation time decreased from 27 to 20 min. Because of the nature of the nanofiber electrospinning process where the nanofiber covers the surface of sol and consequently decelerates the solvent evaporation, 40 μL of base with 2 mL of stock solution is more preferable for the nanofiber electrospinning process in which a 30 min electrospinning window is desired.

Table 1. Chemical Composition of the TEOS/Glycerol/Ethanol Sol Stock Solution Used for Base-Catalyzed Gelation

	TEOS	glycerol	ethanol	DI H_2O	HCl (1 M)	NH_4OH (1 M)
vol. (mL)	14.4 ± 0.1	51.2 ± 0.1	29.0 ± 0.1	4.1 ± 0.1	0.5 ± 0.1	2.0 ± 0.1
mass (g)	13.4 ± 0.1	64.0 ± 0.1	22.9 ± 0.1			
mole (mmol)	64.6	695.0	496.7	255.6	0.5	2.0
molar ratio	1.0	10.8	7.7	4.0	7.7×10^{-3}	3.1×10^{-2}
concn (mol/L)	0.64	6.9	4.9		4.9×10^{-3}	2.0×10^{-2}

Table 2. Silanol-Terminated PDMS Oligomer Incorporated in the TEOS Sol Solution

oligomer	viscosity (cSt)	M_n(reported)	% OH	M_n(tested)	PDI
DMS-S12	16–32	400–700	4.5–7.5	538	1.425
DMS-S14	35–45	700–1500	3.0–4.0	1350	1.353
DMS-S15	45–85	2000–3500	0.9–1.2	2973	1.769

Table 3. Base (1 M NH_4OH/Ethanol)-Catalyzed TEOS/PDMS Copolycondensation Gelation Time Data (40 μL of Base in 2 mL of Sol)

	gelation time for PDMS (min)			
	20%	30%	40%	50%
DMS-S12	70 ± 1	18 ± 1	31 ± 1	33 ± 1
DMS-S14	30 ± 1	30 ± 1	30 ± 1	30 ± 1
DMS-S15	15 ± 1	20 ± 1	18 ± 1	18 ± 1

The composition of the stock sol solution for this two-stage acid–base-catalyzed sol–gel process is analyzed in Table 1.

PDMS Hybrid Sol–Gel Process. Three silanol-terminated PDMS oligomers were selected; their molecular weights and polydispersity indexes (PDIs) are summarized in Table 2. The PDMS hybrid sol was prepared as follows: into 2 mL of a TEOS sol solution was added a PDMS oligomer (the weight percentage of the PDMS oligomer with respect to the total weight of a TEOS/silane monomer and PDMS in every 2 mL of a TEOS sol solution was varied from 20% to 50%, as shown in Table 4), and the solution was vigorously stirred for 30 min; then 40 μL of base was added, the gelation kinetics of the solution was immediately tested, and the gelation time data of the sol with different weight percentages of the PDMS oligomer are shown in Table 3. As shown in this table, the gelation time windows of the sols with different types and weight percentages of the PDMS oligomers are within 30 min except the one with 20% of DMS-S12. Figure 3 is a series of gelation kinetics plots of the TEOS sol with four different weight percentages of DMS-S15. As shown in this figure and Table 3, with the incorporation of a PDMS oligomer in the sol, the base-catalyzed gelation process of the hybrid sol solution is smooth and well-controlled, allowing a sufficient time window for the nanofiber electrospinning process to embed nanofibers into the sol while it undergoes copolycondensation between PDMS and hydrolyzed TEOS monomers.

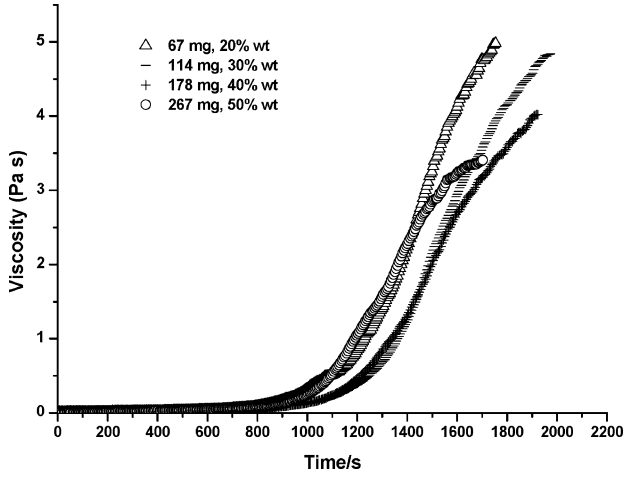

FIGURE 3. Base-catalyzed PDMS-S15/TEOS/glycerol/ethanol sol gelation kinetics.

2.4. Wet-Gel Film Preparation and Nanofiber Electrospinning. After the sol was prepared, it was immediately cast into film form and nanofibers were electrospun into the cast film. Pure Elast-Eon 2A (E2A) and a 50 wt % E2A/poly(ethylene oxide) (PEO) blend were dissolved in *N*,*N*-dimethylformamide (DMF) to form 10 and 7.5 wt % concentrations, respectively. The mixing was performed in a Thinky Mixer at 1600 rpm for 2 h. Electrospinning was performed at 7 kV with 7 cm distance from the tip of the nozzle to the PEO film substrate to form a nanomat film first and, subsequently, impregnated with the sol liquid, forming a gelled film embedded with nanofibers. In the 7.5% (wt % of total polymer in DMF) PEO/PU (50:50 wt %) nanofiber electrospinning experiments, the amount of fiber per unit spinning time was quantified as 0.5 mg/min. After nanofiber incorporation into the sol, the weight percentage of nanofiber with respect to the total weight of silane and a silanol-terminated PDMS oligomer was 1.9%.

2.5. Aging and Solvent Exchange. After gelation of the nanofiber-embedded sol films, the wet-gel film was allowed to age for 24 h at 25 °C and then washed with 20 mL of ethanol three times, in a 12 h cycle each time. The solvent-exchange method allowed us to remove nearly all of the glycerol-containing fluid before drying.

2.6. SCF Drying. SCF extraction was performed with CO_2 in a 1 L Speed-SFE Chamber (Applied Separations) at NASA Glenn Research Center. The wet-gel films were placed in a 1 L SCF extraction chamber, where the ethanol was exchanged with liquid CO_2 at approximately 100 bar and 25 °C in five 2 h cycles. Heating the chamber to 45 °C caused the pressure to increase to around 215 bar, converting the liquid CO_2 to a supercritical state. Slow controlled venting of the chamber gave an aerogel film with 35 mm diameter and 1 mm thickness.

2.7. Characterization. The planar and cross-sectional images of the nanofiber-reinforced silica film were observed using a scanning electron microscope (JSM 7401F-7401). Solid ^{29}Si NMR was performed on a Varian NMR System NB500, and ^{29}Si NMR chemical shifts were corrected by using 3-(trimethylsilyl)-1-propanesulfonic acid sodium salt (^{29}Si = 1.46 ppm) as an external reference. A confocal laser scanning microscopy (LSM) image was performed on a Zeiss LSM 5 exciter. Brunauer–Emmett–Teller (BET) measurements were carried out on Micromeritics ASAP2020 to obtain the specific surface area, pore volume, and pore-size distribution of the prepared samples with N_2 gas adsorption and desorption. The three-point flexural bending tests were done using an Instron 5543 testing machine in the flexural mode. The test fixture used for the flexural tests, in conjunction with the Instron machine, is shown in Figure 4. The span between the lower point contacts was 25.0 mm, with a 4.9 N force load cell and a 50 mm/min crosshead speed.

The equations used to calculate the flexural stress (σ_f), flexural strain (ϵ_f), and flexural modulus (E_f) are as follows:

$$\sigma_f = \frac{3PL}{2bd^2} \quad \varepsilon_f = \frac{6\Delta d}{L^2} \quad E_f = \frac{L^3P}{4bd^2\Delta}$$

where P is the applied load, L is the sample span, b is the sample width, d is the sample thickness, and Δ is the sample deflection.

The density and thermal characterization of the samples were performed at Thermo Physical Research Laboratory. Thermal diffusivities (α) of the samples were measured by the laser flash method (ASTM E1461). Bulk density (d) values were determined from the geometries and masses of the samples. Specific heat (c_p) values were measured using a differential scanning calorimeter, and the thermal conductivity (k) was calculated as a product of these quantities, i.e., $k = \alpha c_p d$.

In the flash method, the front face of a small disk-shaped sample is subjected to a short laser burst and the resulting rear-face temperature rise is recorded and analyzed. The apparatus consists of a Korad K2 laser, a high-vacuum system including a bell jar with windows for viewing the sample, a tantalum or stainless steel tube heater surrounding a sample holding assembly, a thermocouple or an IR detector, appropriate biasing circuits, amplifiers, A/D converters, crystal clocks, and a computer-based digital data acquisition system capable of accurately taking data in the 40 μs and longer time domain. The sample surface was sprayed with a thin layer of heat-resistant black paint in order to increase the surface emissivity and to prevent the IR detector from "seeing" through or into the sample material. Samples were attached to a thin ($L = 0.1218$ cm) graphite A layer, which was facing a laser beam during the experiment, and the thermal diffusivity values were calculated using a two-layer program.

The specific heat was measured using a standard Perkin-Elmer model DSC-2 differential scanning calorimeter with sapphire as the reference material (ASTM E1269). The standard and sample were subjected to the same heat flux as a blank, and the differential powers required to heat the sample and standard at the same rate were determined using the digital data acquisition system. From the masses of the sapphire standard and sample, the differential power, and the known specific heat of sapphire, the specific heat of the sample was computed. The experimental data are visually displayed as the experiment progresses. All measured quantities are directly traceable to NIST standards.

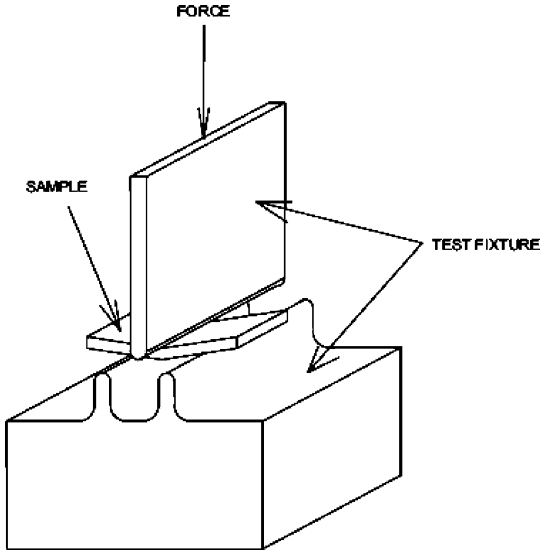

FIGURE 4. Schematic of the three-point bending text fixture for the Instron tester.

3. RESULTS AND DISCUSSION

There are three major aspects in the nanofiber electrospun aerogel (xerogel) synthesis process: (1) the chemical composition of the sol and the gelation kinetics of the sol–gel process; (2) the type and composition of nanofiber-forming material(s); (3) the interaction of the sol component with the nanofiber during the gelation and the subsequent aging and washing processes. These three main factors provide us with a substantial opportunity to manipulate the microstructure, morphology, and therefore the consequent physical and mechanical properties of the final reinforced aerogel (xerogel) product.

TEOS was used as the basic inorganic component because of its controllable hydrolysis and condensation rates. It can assist in incorporating oligomeric species into the system. In order to improve the flexibility of the aerogel film, silanol-terminated PDMS was chosen to be the oligomeric component because of the similarity of its backbone structure (–SiO–) with the sol–gel glass matrix of TEOS and also because of its good thermal stability. Another feature of silanol-terminated PDMS oligomers is that the terminal silanol groups render PDMS susceptible to condensation under both mild acid and base conditions. This feature facilitates the copolycondensation of PDMS with a hydrolyzed TEOS monomer in the base-catalyzed gelation step of this two-stage sol–gel process. PDMS oligomer functions as an additive, modifying the high stiffness and brittleness of a silica aerogel by the mechanism of elastomer reinforcement and giving toughness and flexibility to the product. In this work, we systematically studied how the amount of the oligomer added and the oligomeric molecular weight affect the morphology and physical properties of the aerogel films. The preliminary results show that although brittleness is still present, depending upon the oligomeric level, the flexibility is much improved over that of the pure TEOS sol–gel glasses.

A PU-containing PDMS in the soft-segment Elast-Eon TM E2A was chosen as a reinforcing nanofiber. With use of the electrospinning process, the nanofibers are dispersed readily into the fresh cast sol and incorporated in the gel network during the gelation process. These PU copolymers are expected to form compatibility with the gel network, add flexibility through its soft segments, and add strength through its hard PU segments. In the PDMS hybrid sol–gel process, a polymer blend composed of E2A and PEO was employed to produce the nanofiber. PEO/PU can be dissolved in DMF to form a homogeneous solution before phase separation in 24 h. This gives us sufficient time for the electrospinning of homogeneous blend nanofibers. PEO was utilized in the PU blend to improve the wetting behavior by the hydrophilic TEOS sol.

Two key points determine the success of the nanofiber incorporated sol–gel process: one is the initial viscosity of the sol, and the other is the gelation time window after the addition of a condensation catalyst. The viscosity of the sol

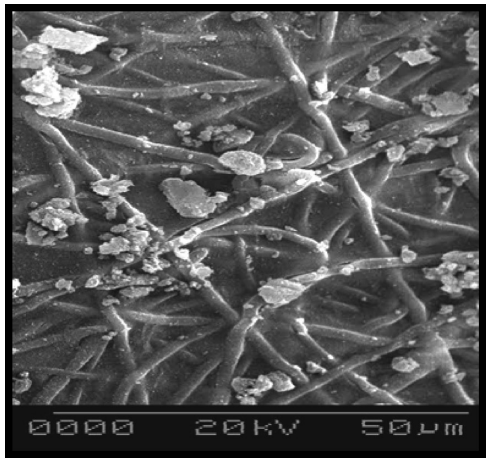

FIGURE 5. SEM micrograph of a silica aerogel film reinforced with E2A fibers.

at the time of casting is related to the aerogel (xerogel) density and film thickness. A suitable precursor sol for aerogel (xerogel) casting and nanofiber electrospinning should allow control of the film thickness and aerogel (xerogel) density and be relatively stable prior to deposition of the gel relatively soon after casting and electrospinning. In this work, a multisolvent glycerol/ethanol was employed in the synthesis of the sol. Glycerol was chosen to control the initial sol viscosity, whereas the volatile ethanol was selected as a cosolvent because its fast evaporation is required to facilitate the onset of gelation (8). Another attractive feature of glycerol is that at ambient temperature its evaporation rate is sufficiently low so that several hours at ambient conditions will not yield significant pore collapse or dramatic shrinkage of the films. It is desirable that the gel point is reached as soon as possible after casting and nanofiber deposition is finalized. In this work, a 30 min electrospinning window was acquired by adjusting the amount of base catalyst, i.e., 40 μL of a 1 M NH_4OH/ethanol solution in 2 mL of a stock solution.

Pure TEOS Aerogel Reinforced by a E2A PU Fiber. Figure 5 shows scanning electron microscopy (SEM) micrographs of the reinforced silica aerogel film. This film was prepared from a pure TEOS sol without silanol-terminated PDMS oligomer added, and the reinforcing fiber is a E2A PU copolymer. As can be seen from the image, the fibers are uniformly dispersed and incorporated in the silica aerogel matrixes. There is a seamless boundary between the aerogel and fibers. Figure 6 shows the top view of the sample fractured. Looking down the crevasse, we observe that a large number of unbroken nanofibers are crisscrossing it. This indicates that the nanofibers are well-embedded in the silica aerogel film.

TEOS/DMS-S14 Hybrid Xerogel Reinforced by PEO/PU Blend Polymer Fibers. On the basis of the results of pure TEOS/glycerol/ethanol sol with a E2A fiber, we further look into the reinforcement effect of a fiber made from a polymer blend PEO/E2A with a 50:50 weight percentage ratio. In this case, a PDMS oligomer (DMS-S14) incorporated sol (30 wt %) was employed. The nanofiber precursor solution was made by 7.5% PEO and E2A (50:50

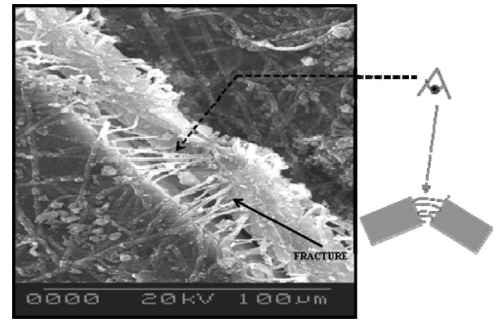

FIGURE 6. SEM micrograph of a fractured silica aerogel film reinforced with E2A fibers.

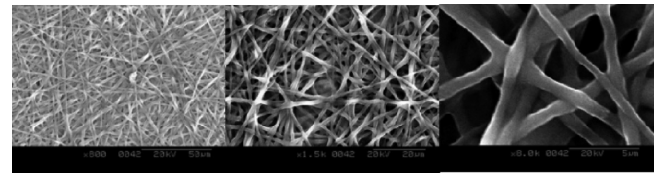

FIGURE 7. PU (E2A)/PEO polymer blend fiber SEM images at three magnification levels.

wt %) in DMF. As shown in Figure 7, the fibers are well produced by the electrospinning process with 500 nm diameter. A multilayer xerogel wet film was made with the procedure depicted in the Experimental Section and aged in a sealed container for 4 days; then the pore fluid was exchanged with 20 mL of fresh ethanol overnight and then washed with fresh ethanol three times for 6 h with 20 mL every 2 h. The sample was then left in 20 mL of hexane in a closed container overnight and air-dried to obtain a PDMS hybrid TEOS-based xerogel film.

As the film was cast onto a poly(ethylene terephthalate) (PET) carrier, the front side was exposed to air and fresh ethanol for pore fluid exchange, while the reverse side was in touch with the PET carrier. The morphology developed on these two sides is significantly different. As shown in Figure 8, the fiber network provides support of the xerogel infrastructure. The polymer-blend fibers on the surface experience capillary disruption and form well-connected pearl-necklace beads because of the ethanol dissolution of the PEO phase during the solvent-exchange and washing steps. On the other hand, SEM images of the reverse side (Figure 9) of the sample indicate that fibers that are embedded preserve their fiber form because of the confinement effect in the matrix.

As shown in Figure 9, there is phase separation in this copolymerized system. In this particular system, the 30% PDMS-S14 with respect to the total weight of TEOS and PDMS is equivalent to a 6.2% molar percentage of total moles of PDMS and TEOS in the system. The regularly distributed macropores with ca. 20 μm diameter are knit by the nanofibers. More interestingly, compared to Figure 5, where the shape of the fibers is linear, the nanofibers in Figure 9 display a network structure in the form of fibrils approximating that of a helix. In this structure, because of the formation of a network of regularly distributed helix-shaped strings, the nanofiber and the silica particles cannot be differentiated from one another. We attribute the forma-

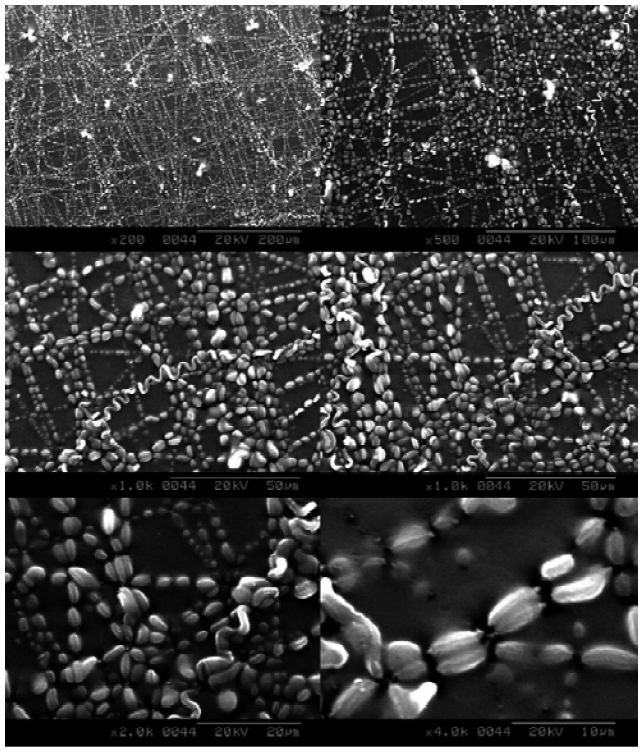

FIGURE 8. SEM images of the front side of the E2A/PEO nanofiber-reinforced multilayer xerogel film.

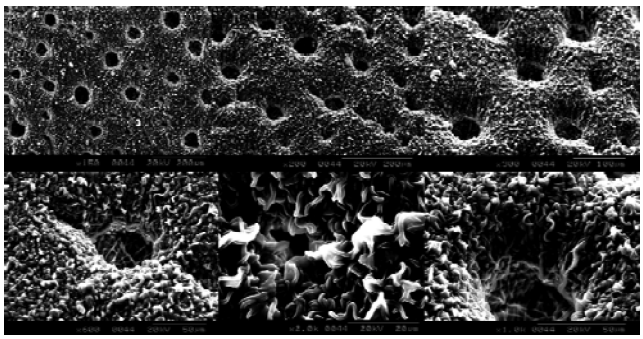

FIGURE 9. SEM images of the reverse side of the E2A/PEO nanofiber-reinforced multilayer xerogel film.

tion of this homogeneous network structure to the occurrence of multiple factors during gelation. First, the PEO phase of the nanofibers that penetrate deep into the silica sol during the electrospinning process are dissolved in the glycerol/ethanol/H_2O cosolvent environment of the sol. In the meantime, the sol impregnates the etched space, and the fibers and the development of the TEOS/PDMS copolycondensation particles occur along the helix of the fibers. The overall effect of this partial nanofiber dissolution and silica particle invasion is the formation of a network of regularly distributed helix-shaped strings, in which the nanofiber and the silica particles forms a single entity and cannot be differentiated. This phenomenon suggests that phase separation and dissolution of the outer-layer component of the fibers provide more intimate contact between the fibers and the sol and direct the silica particle and subsequent whole network growth and expansion of the film. Figure 10 shows the SEM images of a crack formed during the air-drying process. The homogeneous TEOS/fiber

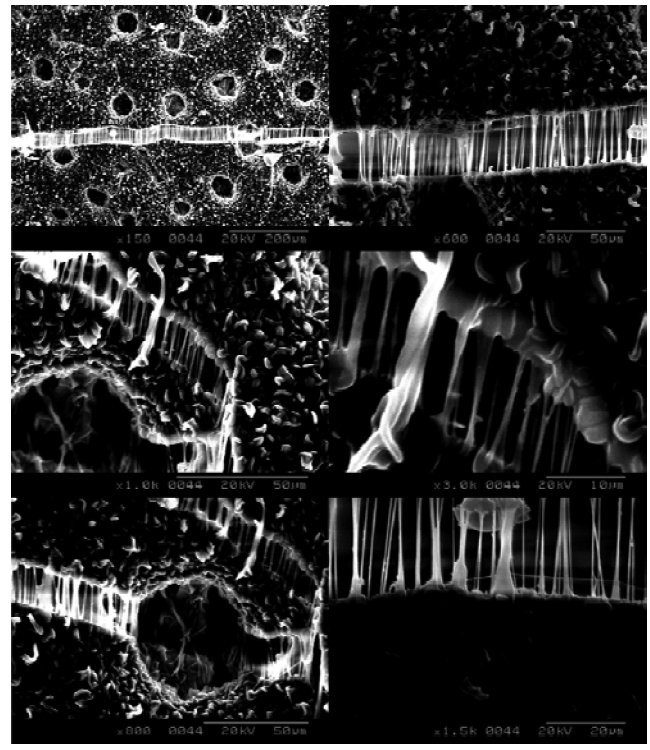

FIGURE 10. SEM images of the crack on the reverse side of the xerogel film.

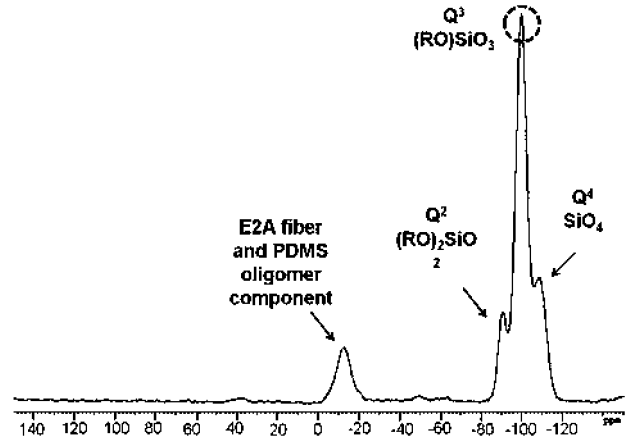

FIGURE 11. Solid-state ^{29}Si NMR plot of a DMS-S14 (30 wt %) /TEOS/glycerol/ethanol hybrid xerogel.

morphology becomes apparent in the crack line perpendicular to the crack when they are pulled out due to crack formation. Additionally, it is worthwhile to mention that the weight percentage of the nanofiber is less than 2% with respect to the total weight of the PDMS oligomer, TEOS monomer, and embedded nanofiber in the film. Figure 11 shows the ^{29}Si NMR plot of this xerogel. The spectrum shows the expected Si−O−Si signals at −90, −100, and −109 ppm. These were assigned to partially condensed $Q^2(RO)_2SiO_2$ and $Q^3(RO)SiO_3$ and fully condensed $Q^4(SiO_4)$ species. The peak at −12 ppm is due to the $-O^{29}Si(CH_3)_2O-$ signal of the PDMS component coming from the soft segment of the E2A reinforcing nanofiber and PDMS oligomer participating in the cocondensation with TEOS during the sol−gel process.

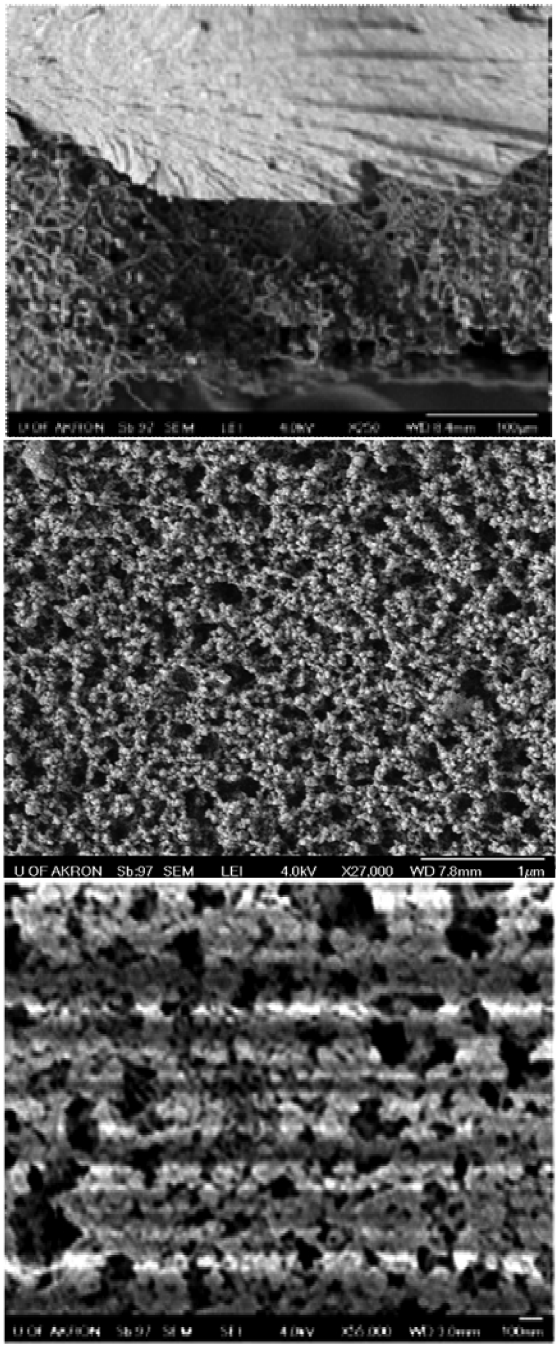

FIGURE 12. SEM image of 50% DMS-S12/TEOS aerogel reinforced with E2A fiber.

PDMS/TEOS Hybrid Aerogel Reinforced by a E2A PU Fiber. In contrast to the pure TEOS-based aerogel, the hydrophobicity of the PDMS oligomer component in the sol solution prevents the electrospun fibers from penetrating into the sol and results in the physical separation of the fibers and the sol solution. Figure 12 shows an aerogel sample with 50% DMS-S12 with respect to TEOS. As shown in this figure, the fibers are not incorporated in the silica matrixes, resulting in one distinct fiber layer separated from the silica layer. The silica particle size is of ca. 30 nm (middle picture), and the size of the particle aggregate is around 100 nm (bottom picture).

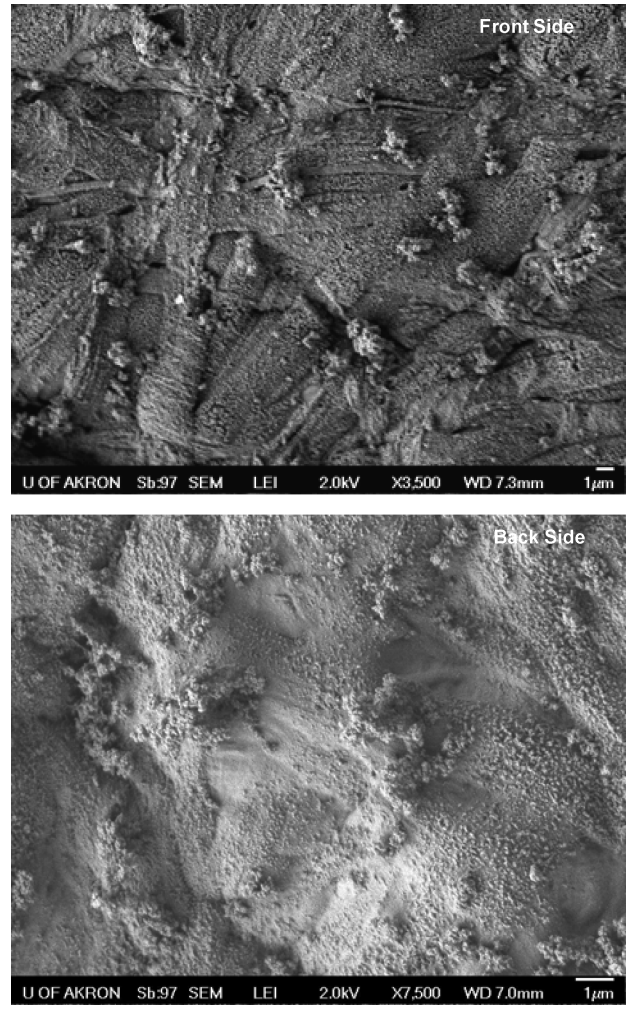

FIGURE 13. SEM images of 20% DMS-S15 reinforced with a (50:50 wt %) PU/PEO fiber.

PDMS/TEOS Hybrid Aerogel Reinforced by a PU/PEO Polymer Blend Fiber. In order to improve the hydrophilicity of the fibers, the PU/PEO polymer blend was used in the PDMS/TEOS sol–gel process. Figure 13 shows the SEM image of an aerogel sample made from the sol with 20% DMS-S15 reinforced with a PU/PEO fiber. The top and bottom images are the front and back sides of the film, respectively. As shown in this figure, the fibers are well embedded in the silica network with a seamless boundary between the aerogel and fibers. The impressions of the fibers covered by the aerogel layer can be noticed in these films.

Figure 14 shows the confocal LSM image of the same aerogel sample. This figure illustrates the rough surface topography. The roughness of the surface is around 4 μm. The average peak width detected by the laser beam is 350 nm, which is the average size of silica particle aggregates and smaller than the electrospun fiber diameter, i.e., around 1 μm in this sample. These LSM data point out that the fibers are well incorporated into the silica network, which are in line with the facts shown in the SEM images. Table 4 summarizes the shape and composition of the TEOS/PDMS hybrid wet film dried after SCF drying. As shown in this table, for the highest molecular weight of the silanol-

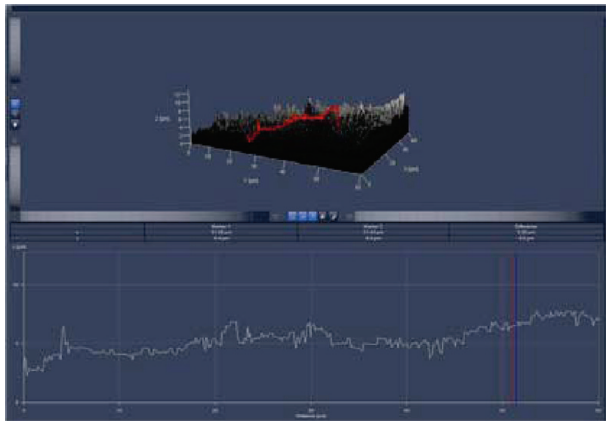

FIGURE 14. Confocal LSM image of 20% DMS-S15 reinforced with a (50:50 wt %) PU/PEO fiber.

terminated PDMS oligomer, the film shrinkage occurrs (DMS-S15, 20 wt %), and with the weight percentage increased, the hybrid film cracked. This suggests that the longer chain of the flexible PDMS oligomer renders greater collapse of pores to occur, whereas the aerogel samples containing a medium-sized PDMS oligomer were maintained as intact films after SCF drying without pore collapse and film shrinkage.

The surface area and pore structure of selected samples in Table 4 were examined with BET measurements, and the data are summarized in Table 5. The mesoporosity (pores with diameters in the range of 2−50 nm) of all of the nanofiber-reinforced hybrid films was confirmed by N_2 physisorption measurements, with the average pore diameter of ca. 11 nm calculated by the BET method. In addition, as shown in Table 5, the amount and type of fiber incorporated in the film and the molecular weight of the PDMS oligomer have little influence on the pore size of the aerogel matrix. As calculated by the BET method, all of these mesoporous films have high surface areas in the range of 600−760 m^2/g, which are typical values for silica aerogel. There is no significant influence of the amount of the PDMS oligomer and the type of nanofiber on the BET surface area at a low-molecular-weight PDMS oligomer. However, with the PDMS chain length increase combined with higher weight percentage in the silica matrix, the surface area increased around 16% by comparing film D with film C. Pore-size distribution plots of films A−E (Figure 15) calculated by the Barrett−Joyner−Halenda (BJH) method from the desorption branch suggest the presence of a broad range of pore sizes in the meso- and macropore (pore diameter >50 nm) size regions, which is consistent with the aerogel nature.

Table 5. BET Surface Area and Porosity Data of Selected Samples in Table [4]

sample	BET surface area (m^2/g)	average pore diameter (BET, nm)	BJH adsorption cumulative pore volume (cm^3/g)
film A	652.18 ± 1.26	11.3	2.29
film B	648.67 ± 1.32	11.4	2.32
film C	617.32 ± 1.34	12.5	2.33
film D	759.35 ± 1.41	11.6	2.78
film E	755.42 ± 1.18	11.5	3.07
film F	604.46 ± 2.32	22.56	3.40

Mechanical Properties of a Hybrid Aerogel Reinforced by a PU/PEO Polymer Blend Fiber. Aerogel samples of thick sheets (~2 mm) and thin films (~0.5 mm) showed substantial stability and robustness during bending tests. The picture in Figure 16a shows a thick aerogel sheet flexed in the three-point text fixture of the Instron tester. The picture was taken after halting the experiment halfway through a complete bending cycle. As shown in the picture, the thick sheet can undergo considerable bending.

A thinner aerogel hybrid composite film that could be flexed to almost 180° with a steep curve is shown in Figure 16b.

Careful observation of the samples after mechanical tests evidence that the nanofiber component is primarily responsible for the ability of the samples to bend without breaking. In fact, the aerogel component of the composite itself is still not flexible enough at the molecular level to exhibit such high levels of flexing. One can still observe the formation of cracks, especially for thick samples after considerable bending. The cracks that form after bending, however, are held together tightly by the nanofibrous network that is anchored to the aerogel layer. This, in turn, prevents disintegration of the entire hybrid film during bending. In order to demonstrate this effect, we have purposely created large cracks in our aerogel sheets by complete folding of the sheet and pulling apart gently to separate the gaps between the cracks. As one can see in Figure 17, gaps between the cracked aerogel sections are bridged by the nanofibers, preventing them from disintegrating. The crack size in the picture is around 20 μm, much larger than is typically observed under normal bending and flexing conditions. As the thickness decreases from the sheet (2 mm) to film (0.5 mm) range, the cracks are very minimal and those that occur are very small, 5 μm.

The average flexural mechanical properties of the aerogel films are summarized in Table 6.

Table 4. Shape and Form of a Multilayer TEOS/PDMS Hybrid Wet Film Dried after SCF Drying

	DMS-S12 (M_n = 538)		DMS-S14 (M_n = 1350)		DMS-S15 (M_n = 2973)
	PU fiber	PU/PEO fiber	PU fiber	PU/PEO fiber	PU/PEO fiber
134 mg (20%, wt %)	intact film	intact film	intact film	intact film, film C	intact film with shrinkage
228 mg (30%, wt %)	intact film, film A	intact film	intact film	intact film	cracked film
356 mg (40%, wt %)	intact film, film B	intact film	intact film	intact film, film D	cracked film
534 mg (50%, wt %)	intact film	intact film, film F	intact film	intact film, film E	cracked film

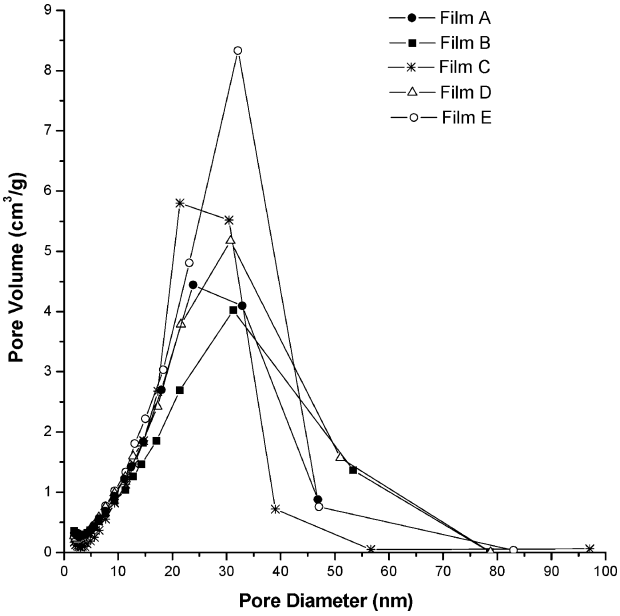

FIGURE 15. Pore-size distribution plots of films A–E.

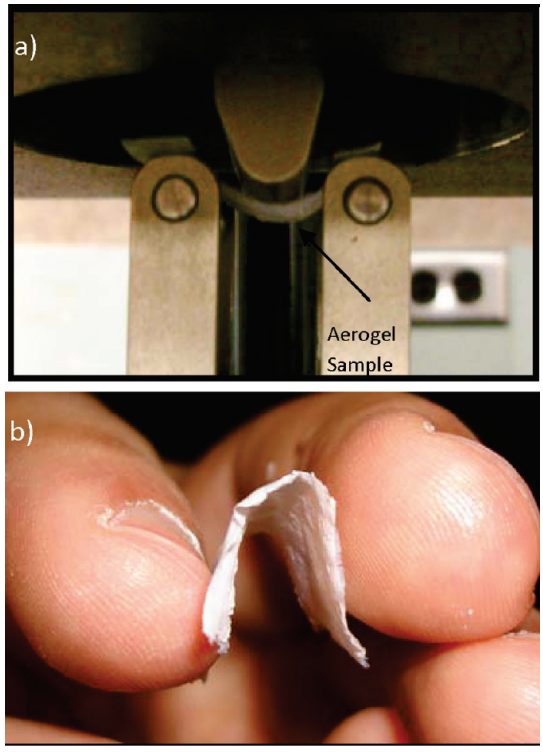

FIGURE 16. (a) 80-mil-thick aerogel–nanofiber hybrid sheet flexing during the bending test. (b) 0.46-mm-thick aerogel–nanofiber hybrid film bent almost 180° (film sample D in Table 4).

After incorporating the nanofibers in the aerogel films, we were also interested in determining whether the nanofiber-reinforced aerogels still display low thermal conductivity and density, typical of a pristine silica aerogel. The average specific heat results of the hybrid aerogel films are given in Table 7. The dimensions, masses, and bulk densities of the two film samples D and F (see Table 4) used for thermal diffusivity and conductivity measurements are given in Table 8. The total relative expanded uncertainty (coverage factor $k = 2$) of the specific heat and density determination is around ±3%. The total compound expanded uncertainty ($k = 2$) of the thermal conductivity determination is ±10%.

The thermal diffusivity and conductivity of the hybrid film samples D and F are tabulated in Tables 9 and 10, respectively. According to these results, the nanofiber-reinforced aerogel films still display very low conductivity and density. This is due to the low concentration of nanofibers. In addition, as shown in Table 10, the thermal conductivity of the lightweight (0.172 g/cm^3) film F is as low as that of the pristine silica aerogel (13 mW/m·K), whereas the thermal conductivity of film D (0.079 g/cm^3) is twice as much as that of air (26 mW/m·K) and comparable to that of glass wool (40 mW/m·K) or PU foam (24–30 mW/m·K) (31, 32). The

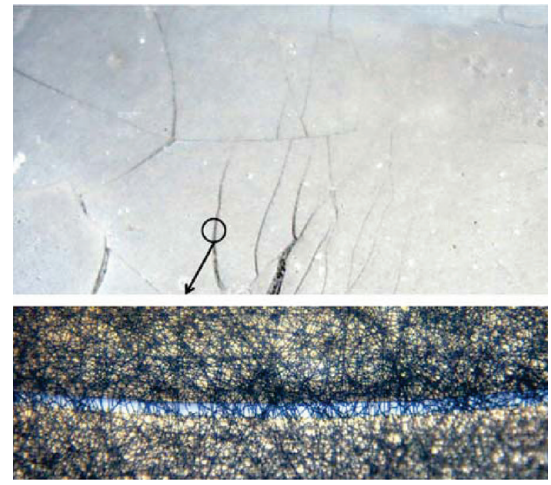

FIGURE 17. 80-mil-thick aerogel sheet after excessive repetitive bending and pulling apart by hand.

Table 6. Flexural Mechanical Properties

flexible modulus (MPa)	max flex stress (kPa)	flex strain at yield (%)
5–10	150–200	8–10

Table 7. Specific Heat Values

T (°C)	c_p (J/g·K)	T (°C)	c_p (J/g·K)
20	0.969	80	1.135
30	1.002	90	1.158
40	1.032	100	1.180
50	1.058	110	1.203
60	1.087	120	1.224
70	1.111		

Table 8. Sample Dimensions, Masses, and Density Values

film	thickness (cm)	width (cm)	length (cm)	mass (g)	density (g/cm^3)
D	0.0462	1.314	1.327	0.006 38	0.079
F	0.0857	1.264	1.307	0.024 33	0.172

Table 9. Thermal Diffusivity at Different Temperatures

	α (cm^2/s)	
T (°C)	film D	film F
20	0.006 58	0.000 77
50	0.005 86	0.000 82
100	0.005 53	0.000 80

Table 10. Thermal Conductivity at Different Temperatures

	k (mW/m·K)	
T (°C)	film D (40 wt %, DMS-S14, $M_n = 1350$)	film F (50 wt %, DMS-S12, $M_n = 538$)
20	50.5	12.9
50	49.1	14.9
100	51.7	16.2

difference in the thermal conductivity between the two samples lies in the molecular weight and the weight percentage of the PDMS oligomer participating in the cocondensation polymerization of TEOS within the silica matrix. The result shows that a higher weight percentage of the PDMS oligomer with lower molecular weight forms better uniformity within the silica aerogel network with more evenly distributed mesoporosity, therefore rendering low thermal conductivity comparable to the pristine silica aerogel with a slight density penalty.

CONCLUSIONS

We have implemented a novel hybrid film casting/electrospinning process (30) to produce continuous polymer nanofiber-reinforced aerogels/xerogels. To our knowledge, this is the first reported synthesis method of an in situ electrospun nanofiber-reinforced aerogel/xerogel film with controlled silica sol gelation kinetics. BET results showed that the mesoporous PDMS-modified hybrid aerogels reinforced by PU/PEO nanofibers have high surface area and large pore volume. SEM results show that the nanofibers are well incorporated and dispersed in the silica film. There is a seamless connection between the fibers and silica matrixes. Owing to the well-integrated nanofibrous network within the aerogel phase, the hybrid aerogel films are repeatedly bendable. The aerogel phase, though still not inherently flexible, possesses all of the other useful attributes of pristine aerogels, i.e., high porosity, low thermal conductivity, etc. These, combined with the bendable nature of the entire composite film brought about by the nanofibers, render these films useful for applications that require flexing, wrapping, and rolling.

REFERENCES AND NOTES

(1) Lu, X.; Arduini-Schuster, M. C.; Kuhn, O. N. J.; Fricke, J.; Pekala, R. W. *Science* **1992**, *255*, 971–972.
(2) Brinker, C. J.; Scherer, G. W. *Sol–Gel Science*; Academic Press Inc.: New York, 1990.
(3) Aguado-Serrano, J.; Rojas-Cervantes, M. L. *Microporous Mesoporous Mater.* **2006**, *88*, 205–213.
(4) Pierre, A. C.; Pajonk, G. M. *Chem. Rev.* **2002**, *102*, 4243–4265.
(5) Goda, H.; Frank, C. W. *Chem. Mater.* **2001**, *13*, 2783–2787.
(6) Rao, A. V.; Bhagat, S. D. *Solid State Sci.* **2004**, *6*, 945–952.
(7) Kim, S. M.; Charrabarti, K.; Oh, E. O.; Whang, C. M. *J. Sol–Gel Sci. Technol.* **2003**, *27*, 149–155.
(8) Smith, D. M.; Johnston, G. P.; Ackerman, W. C.; Stoltz, R. A.; Maskara, A.; Ramos, T.; Jeng, S.-P.; Gnade, B. E. U.S. Patent 6,380,105, 1999.
(9) Gesser, H. D.; Goswami, P. C. *Chem. Rev.* **1989**, *89*, 765–788.
(10) Leventis, N. *Acc. Chem. Res.* **2007**, *40*, 874–884.
(11) Leventis, N.; Sotiriou-Leventis, C.; Zhang, G.; Rawashdeh, A.-M. M. *Nano Lett.* **2002**, *2*, 957–960.
(12) Katti, A.; Shimpi, N.; Roy, S.; Lu, H.; Fabrizio, E. F.; Dass, A.; Capadona, L. A.; Leventis, N. *Chem. Mater.* **2006**, *18*, 285–296.
(13) Capadona, L. A.; Meador, M. A. B.; Alunni, A.; Fabrizio, E. F.; Vassilaras, P.; Leventis, N. *Polymer* **2006**, *47*, 5754–5761.
(14) Meador, M. A. B.; Capadona, L. A.; McCorkle, L.; Papadopoulos, D. S.; Leventis, N. *Chem. Mater.* **2007**, *19*, 2247–2260.
(15) Zhang, G.; Dass, A.; Rawashdeh, A.-M. M.; Thomas, J.; Counsil, J. A.; Sotiriou-Leventis, C.; Fabrizio, E. F.; Ilhan, F.; Vassilaras, P.; Scheiman, D. A.; McCorkle, L.; Palczer, A.; Johnston, J. C.; Meador, M. A. B.; Leventis, N. *J. Non-Cryst. Solids* **2004**, *350*, 152–164.
(16) Meador, M. A. B.; Fabrizio, E. F.; Ilhan, U. F.; Dass, A.; Zhang, G. H.; Vassilaras, P.; Johnston, J. C.; Leventis, N. *Chem. Mater.* **2005**, *17*, 1085–1098.
(17) Ilhan, U. F.; Fabrizio, E. F.; McCorkle, L.; Scheiman, D. A.; Dass, A.; Palczer, A.; Meador, M. A. B.; Johnston, C. J.; Leventis, N. *J. Mater. Chem.* **2006**, *16*, 3046–3054.
(18) DeFriend, K. A.; Espinoza, B.; Patterson, B. *Fusion Sci. Technol.* **2007**, *51*, 693–700.
(19) Meador, M. A. B.; Vivod, S. L.; McCorkle, L.; Quade, D.; Sullivan, R. M.; Ghosn, L. J.; Clark, N.; Capadona, L. A. *J. Mater. Chem.* **2008**, *18*, 1–11.
(20) Zhang, Z.; Shen, J.; Ni, X.; Li, Y.; Wang, B.; Wu, G.; Zhou, B. *Rare Met. Mater. Eng.* **2008**, *37*, 16–19.
(21) Lee, J. K. U.S. Patent 0,259,979, 2007.
(22) Gunatillake, P. A.; Martin, D. J.; Meijs, G. F.; McCarthy, S. J.; Adhikari, R. *Aust. J. Chem.* **2003**, *56*, 545–557.
(23) Li, L.; Yalcin, B.; Meador, M. A. B.; Cakmak, M. *Polym. Prepr. (Am. Chem. Soc., Div. Polym. Chem.)* **2008**, *49*, 554.
(24) Bognitzki, M.; Czado, W.; Frese, T.; Schaper, A.; Hellwig, M.; Steinhart, M.; Greiner, A.; Wendorff, J. H. *Adv. Mater.* **2001**, *13*, 70–72.
(25) Deitzel, J. M.; Kosik, W.; McKnight, S. H.; Tan, N. C. B.; DeSimone, J. M.; Crette, S. *Polymer* **2002**, *43*, 1025–1029.
(26) Doshi, J.; Reneker, D. H. *Electrostatic* **1995**, *35*, 151.
(27) Reneker, D. H.; Chun, I. *Nanotechnology* **1996**, *7*, 216.
(28) Andrady, A. L. *Science and Technology of Polymer Nanofibers*; John Wiley: New York, 2008.
(29) Reneker, D. H.; Yarin, A. L. *Polymer* **2008**, *49*, 2387–2425.
(30) Cakmak, M.; Reneker, D. H.; Yalcin, B. Patent WO2007047662, 2007.
(31) Kocon, L.; Despetis, F.; Phalippou, J. *J. Non-Cryst. Solids* **1998**, *225*, 96–100.
(32) Schmidt, M.; Schwertfeger, F. *J. Non-Cryst. Solids* **1998**, *225*, 364.

AM900451X